Interpretable Real-Time Modelling of the Diffusion Overpotential in Lithium Batteries

Alan G. Li and Matthias Preindl *Senior Member, IEEE*

***Abstract*—Fractional-order dynamics can form physically-interpretable equivalent-circuit models of the diffusion overpotential in lithium-ion batteries but have complex formulations in the time-domain. Meanwhile, resistor-capacitor circuits have simple implementations but little physical meaning. Thus we propose a discrete-time state-space diffusion model, named 'receding-horizon diffusion' (RHD). It combines physical interpretability with computational simplicity. Analogous to the Warburg element in impedance spectroscopy, the RHD constant is explicitly linked with the lithium ion diffusion coefficient. Fivefold validation of the RHD model using simulated and experimental from lithium NiMnCo and NiCoAl cells up to 3 C-rate, temperatures from 0 to 25°C, and wide ranges of states of health and charge. The model has less than 1% modelling error. Ohmic, charge-transfer, and diffusion overpotentials are tracked in real time. The RHD model could be integrated into battery management systems in electric vehicles and used in standard state estimation techniques.**

***Index Terms*—Batteries, Equivalent circuits, State-space methods, Electrochemical processes**

I. Introduction

Lithium-ion battery (LIB) models form the basis of most battery management systems (BMS) [1]. The BMS depends on accurate models to perform state estimation [2]. Battery models can also be used to provide insight into cell degradation [3], which could allow for advanced degradation-reduction techniques [4]. There are 2 popular model types: physics-based models (PBM) and equivalent circuit models (ECM). PBMs are highly accurate and offer insight into internal cell processes such as equilibrium phases reflected in the OCV, but face challenges in real-time use [5]. ECMs are especially popular in electric vehicle (EV) applications for their simplicity and speed [6] in capturing transport kinetics reflected in the overpotentials. More recently, fractional-order models (FOM) and physically-meaningful ECMs have been proposed that can quantify electrochemical overpotentials in the cell [7]. These models offer greater interpretability than standard ECMs without significantly increasing computation time.

The 'NRC model' is a basic ECM consisting of one series resistor and N pairs of resistors and capacitors in parallel (known as RC pairs), where typically $N > 2$. Estimation and simulation of the model parameters is performed on time-domain voltage data using techniques such as recursive least-squares [8]. Computation of the NRC model is fast due to its linear discrete state-space formulation. The NRC model can predict battery voltage with high accuracy, but lacks interpretability— several RC pairs are used recreate phenomena governed by a single fractional-order process like diffusion. This suffices for a conventional BMS, but tracking and predicting battery overpotentials and degradation is increasingly important for advanced BMS diagnostics [4].

FOMs are a more advanced model used for frequency-domain data obtained through electrochemical impedance spectroscopy (EIS). EIS is a time-consuming process mainly used for laboratory studies [9]. The frequency-varying impedance is modelled with a FOM such as the Randles circuit, whose parameters can be used to provide insight into degradation modes in the cell [10]. FOMs include a constant-phase element (CPE). The CPE is defined by a fractional-order transfer function, which is shown to accurately capture the charge transfer and diffusion overpotentials [11]. In Randles circuits, a 0.5-order CPE named the Warburg impedance is added. FOMs face challenges in BMS implementation because frequency-domain data is difficult to obtain in real-time. Since FOMs can provide insight into overpotentials and degradation, time-domain FOMs have been studied for several years [5], [8], [12], [13]. While the main research focus on FOMs has been identification of the CPE order [14], [15], even simpler fixed-order fractional systems rely on complex formulations such as the short-memory Grünwalde-Letnikov method for discretizing fractional derivatives [5], [8], [12]. This may hinder their widespread use despite their high accuracy and interpretability.

As a likely result of the desire to avoid fractional calculus, overpotential models of diffusion have been combined with NRC elements. Modelling accuracy is increased with additional parameters but without much increase in computational cost [16]. Networks of RC pairs may be assigned to diffusion [17], [18] or a 'diffusion resistance' and 'diffusion time constant' may be introduced [19], [20]. Besides using many parameters, both approaches still fall short in capturing diffusion's fractional-order nature [10]. There remains a need for physically-meaningful ECMs that can describe the diffusion overpotential without sacrificing the interpretability of FOMs.

A. Contributions and outline

A diagram of the methodology of this article is shown in Fig. 1. We propose two novel time-domain definitions of the diffusion overpotential derived from results first obtained in [7]. We name them the 'convolution-defined diffusion' (CDD) and 'receding-horizon diffusion' (RHD) models. They are

This work was supported in part by the Columbia University Data Science Institute Seed Fund Program.

Alan G. Li and Matthias Preindl are with the Department of Electrical Engineering, Columbia University in the City of New York, 500 W. 120th St., Mudd 1310, New York, NY, 10027, USA (e-mail: {agl2142, matthias.preindl}@columbia.edu).

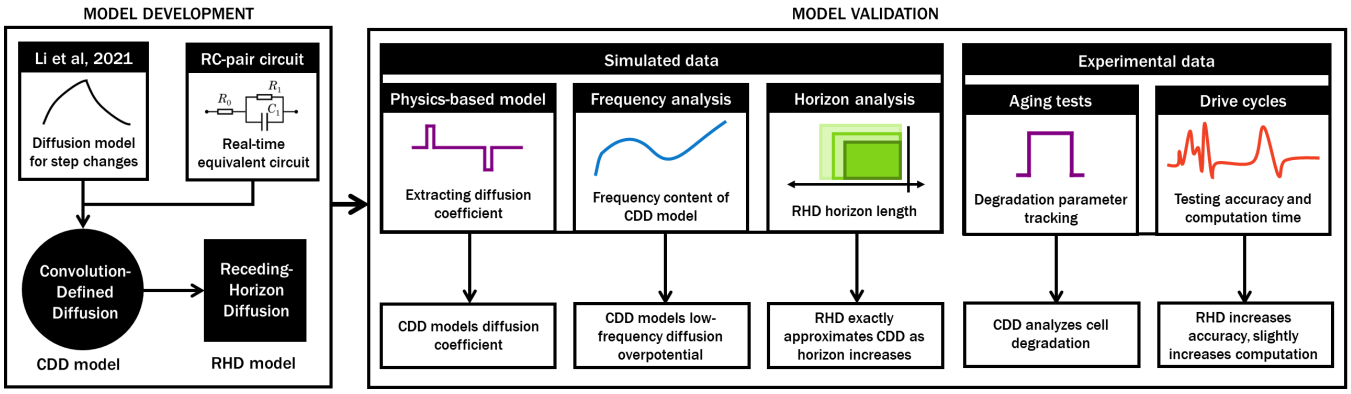

Fig. 1. Diagram representing the structure and methodology of the article, showing development of the CDD and RHD models, validation using simulated and experimental data, and key results.

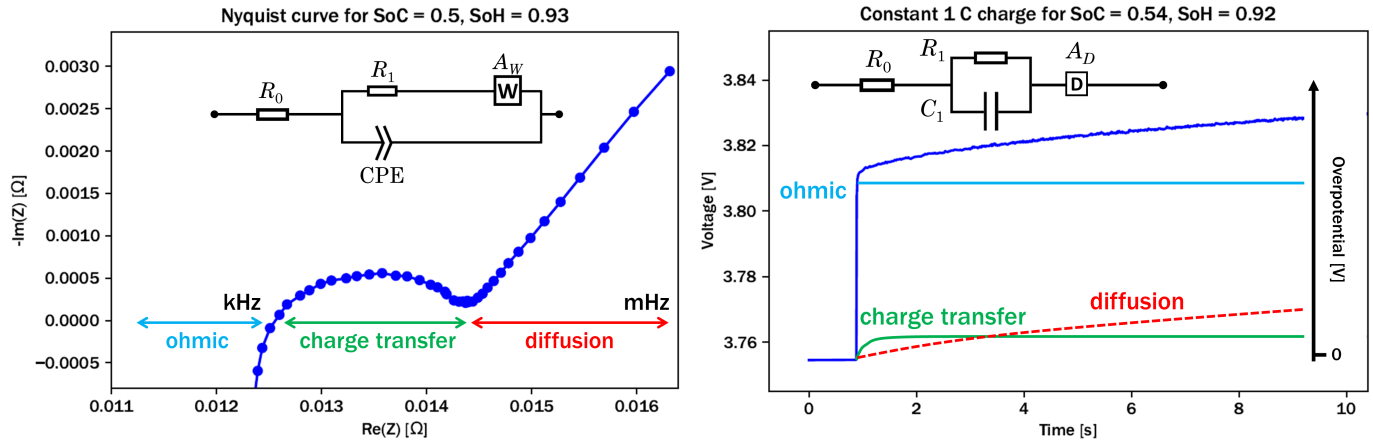

(a) (b)

Fig. 2. Battery equivalent circuits, diagnostics signals, and empirical overpotentials from a Kokam SLPB100216216H NMC cell, showing (a) Fractional-order model (FOM) with a constant-phase element (CPE) and Warburg impedance, and (b) Proposed receding-horizon diffusion (RHD) model

contrasted in Fig. 2 with the frequency-domain FOM model. CDD accurately describes the diffusion overpotential using convolution. RHD approximates CDD using a state-space formulation. Our proposed models offer a discrete-recursive state-space analogue to the Warburg impedance in the time domain using only 1 modelling parameter. The RHD model is accurate, fast, and physically linked to the diffusion coefficient. A standard BMS could easily implement the RHD model to track electrochemical overpotentials in real-time.

Model development is shown in Sections II and III with derivations of the CDD and RHD models. Verification results for the CDD and RHD models are then presented in Sections IV and V using the simulated and experimental methodology shown in Fig. 3. The article is concluded in Section VI.

II. Convolution-Defined Diffusion Model

The CDD model extends galvanostatic intermittent titration principles first described in [7], [21]. Applying Fick's law across a finite-boundary electrode and liquid electrolyte, diffusion is quantified with the diffusion constant A_D [$\mathrm{A}^{-1}\mathrm{s}^{-0.5}$],

$$A_D = \frac{2\beta v_M}{SF\sqrt{D\pi}} \tag{1}$$

TABLE I
Key Electrochemical Parameters.

Symbol	Description	Value	Units
$1/\beta$	Max stoichiometric added lithium	[0, 1]	—
v_M	Molar volume of NMC	$\frac{M_{\mathrm{NMC}}}{\rho_{\mathrm{NMC}}}$	cm^3
M_{NMC}	Molar mass of NMC	96.46	gmol^{-1}
ρ_{NMC}	Density of NMC	4.7	gcm^{-3}
S	Active surface area	$\frac{3\varepsilon_{AM}}{L_{agg}} v_e$	cm^2
ε_{AM}	Volume fraction of active material	[0, 1]	—
L_{agg}	Agglomerate size	—	μm
v_e	Electrode volume	—	cm^3
F	Faraday's constant	96 485	Cmol^{-1}
D	Lithium-ion diffusion coefficient	—	$\mathrm{m}^2\mathrm{s}^{-1}$

where the parameters are defined in Table I. Each current step change at time $t_n \leq t$, $n \in \mathbf{Z}^+$, incites a diffusion state $\psi_n(t)$ [$\mathrm{A \cdot V \cdot s}^{0.5}$] defined as

$$\psi_n(t) = \zeta_n \sqrt{t - t_n} \tag{2}$$

with the diffusion state amplitude ζ_n [$\mathrm{A \cdot V}$] given by

$$\zeta_n = \Delta I(t_n) \nabla V_{OC}(t_n) \tag{3}$$

where we define

$$\begin{aligned}\Delta I(t_n) &= i(t_n) - i(t_n - \Delta t)\\ \nabla V_{OC}(t_n) &= \left.\frac{\partial V_{OC}}{\partial SoC}\right|_{SoC(t_n)}\end{aligned} \tag{4}$$

and where i is the cell current, Δt is the sampling interval, V_{OC} is the open circuit voltage (OCV) and SoC is the state of charge. The DNRC diffusion overpotential is then given by

$$V_{\text{DNRC}}(t) = A_D \sum_{n=1}^{N_{\text{step}}} \psi_n(t) \tag{5}$$

where N_{step} is the total number of step changes.

Those familiar with zero-order hold (ZOH) sampling and the derivation of the Duhamel integral via the superposition of impulses will quickly observe that, as the width of the step changes approaches 0, the DNRC formulation reduces to convolution. Consider the ZOH-modified cell current as a sum of rectangle pulses, denoted by the function rect$(\cdot)$,

$$i(t) = \sum_{k=0}^{\infty} i(t_k) \cdot \text{rect}\left(\frac{t - t_k - \frac{\Delta t}{2}}{\Delta t}\right) \tag{6}$$

Corresponding to each sampling index k are now two step changes in current: the rising and falling edges of the ZOH pulse, which each incite their own diffusion states ψ_k and ψ'_k. The diffusion overpotential becomes

$$V_D(t) = A_D \sum_{k=0}^{\infty} \Big(\psi_k(t) + \psi'_k(t)\Big) \tag{7}$$

Similarly, we have the state amplitude at the rising edge

$$\zeta_k = i(t_k)\nabla V_{OC}(t_k) = \zeta(t_k) \tag{8}$$

which is equal and opposite at the falling edge, $\zeta'_k = -\zeta_k$. Note that ζ is now a function of time. Defining the unit impulse response

$$g_z(t) = \sqrt{t} - \sqrt{t - \Delta t} \tag{9}$$

we see that substituting (8) into (2) yields the sum of the rising and falling edge states

$$\psi_k(t) + \psi'_k(t) = \zeta(t_k) g_z(t - t_k) \tag{10}$$

for $t > t_k$. Substituting (10) into (7) yields convolution, denoted by $*$

$$V_D(t) = A_D \sum_{k=0}^{\infty} \zeta(t_k) g_z(t - t_k) = A_D \cdot \zeta(t) * g_z(t) \tag{11}$$

Thus the diffusion overpotential is represented as a convolution of the diffusion state amplitude ζ with the unit impulse response g_z. Furthermore, the CDD model is linked to FOMs. Taking the continuous Laplace transform $G(s)$,

$$G(s) = \mathcal{L}\left(\lim_{\Delta t \to 0} \frac{g_z(t)}{\Delta t}\right) = \mathcal{L}\left(\frac{1}{2\sqrt{t}}\right) = \sqrt{\frac{\pi}{4}} s^{-1/2} \tag{12}$$

we obtain a fractional-order transfer function. In the time-domain, this becomes a semi-integral which may be calculated with fractional calculus [22].

III. Receding-Horizon Diffusion Model

The full RHD model state equations, including the ohmic V_s and charge transfer V_{ct} overpotentials, are given by

$$\begin{aligned}x(t_{k+1}) &= Ax(t_k) + Bu(t_k)\\ y(t_k) &= Cx(t_k) + \begin{pmatrix}R_0 & 0\end{pmatrix} u(t_k)\end{aligned} \tag{13}$$

$$x(t_k) = \begin{pmatrix}x_\ell(t_k)\\ x_\nu(t_k)\end{pmatrix}, \quad u(t_k) = \begin{pmatrix}i(t_k)\\ i(t_{k-1})\end{pmatrix} \tag{14}$$

$$A = \begin{pmatrix}A_\ell & \mathbf{0}\\ \mathbf{0} & A_\nu\end{pmatrix}, \quad B = \begin{pmatrix}B_\ell\\ B_\nu\end{pmatrix}, \quad C = \begin{pmatrix}C_\ell & C_\nu\end{pmatrix} \tag{15}$$

where the output is linked to the terminal voltage V_o by

$$\begin{aligned}V_o(t_k) &= V_{OC}(t_k) - y(t_k)\\ y(t_k) &= V_s(t_k) + V_{ct}(t_k) + V_D(t_k)\end{aligned} \tag{16}$$

When $N = 2$ RC-pairs are used, the variables A_ℓ, B_ℓ, C_ℓ, and D_ℓ are given by standard NRC equations,

$$\begin{aligned}A_\ell &= \begin{pmatrix}e^{-\frac{\Delta t}{R_1 C_1}} & 0\\ 0 & e^{-\frac{\Delta t}{R_2 C_2}}\end{pmatrix}, \quad B_\ell = \begin{pmatrix}1 - e^{-\frac{\Delta t}{R_1 C_1}} & 0\\ 1 - e^{-\frac{\Delta t}{R_2 C_2}} & 0\end{pmatrix}\\ C_\ell &= \begin{pmatrix}R_1 & R_2\end{pmatrix}\end{aligned} \tag{17}$$

Note that $x_\ell \in \mathbf{R}^N$ is the ohmic and charge transfer state vector, $A_\ell \in \mathbf{R}^{N \times N}$ is a diagonal matrix, $B_\ell \in \mathbf{R}^N$ is a column vector, and $C_\ell \in \mathbf{R}^N$ is a row vector.

The variables x_ν, A_ν, B_ν, and C_ν describe the RHD diffusion element and are formulated below. Rather than convert the DNRC superposition into convolution, we can limit the number of diffusion states by applying a receding-horizon. All states beyond the horizon are assumed to saturate at some constant value. Only states within the horizon are tracked, and an offset term is used to store the saturated states.

We first obtain a discrete-recursive form of a single diffusion state as defined in (2). Due to square-root dynamics, this is a piece-wise function

$$\psi_n(t_{k+1}) = \begin{cases}\psi_n(t_k)\sqrt{1 + \frac{1}{k-n}} & k > n\\ \zeta_n\sqrt{\Delta t} & k = n\\ 0 & k < n\end{cases} \tag{18}$$

Assuming a continuously-varying current input, from (3) and (14) we can define

$$\psi_k(t_{k+1}) = b_\nu(t_k) u(t_k) \tag{19}$$

where $b_\nu(t_k) \in \mathbf{R}^2$ is a row vector dependent on the time step that introduces the OCV gradient and differential current into the RHD model,

$$b_\nu(t_k) = \nabla V_{OC}(t_k)\sqrt{\Delta t}\begin{pmatrix}1 & -1\end{pmatrix} \tag{20}$$

For a horizon with a length of M time steps, the diffusion overpotential becomes

$$\begin{aligned}x_\nu(t_{k+1}) &= A_\nu x_\nu(t_k) + B_v u(t_k)\\ V_D(t_k) &= C_\nu x_\nu(t_k)\end{aligned} \tag{21}$$

$$x_\nu(t_k) = \begin{pmatrix}x_{\text{offset}}(t_k)\\ x_M(t_k)\\ \vdots\\ x_0(t_k)\end{pmatrix} \tag{22}$$

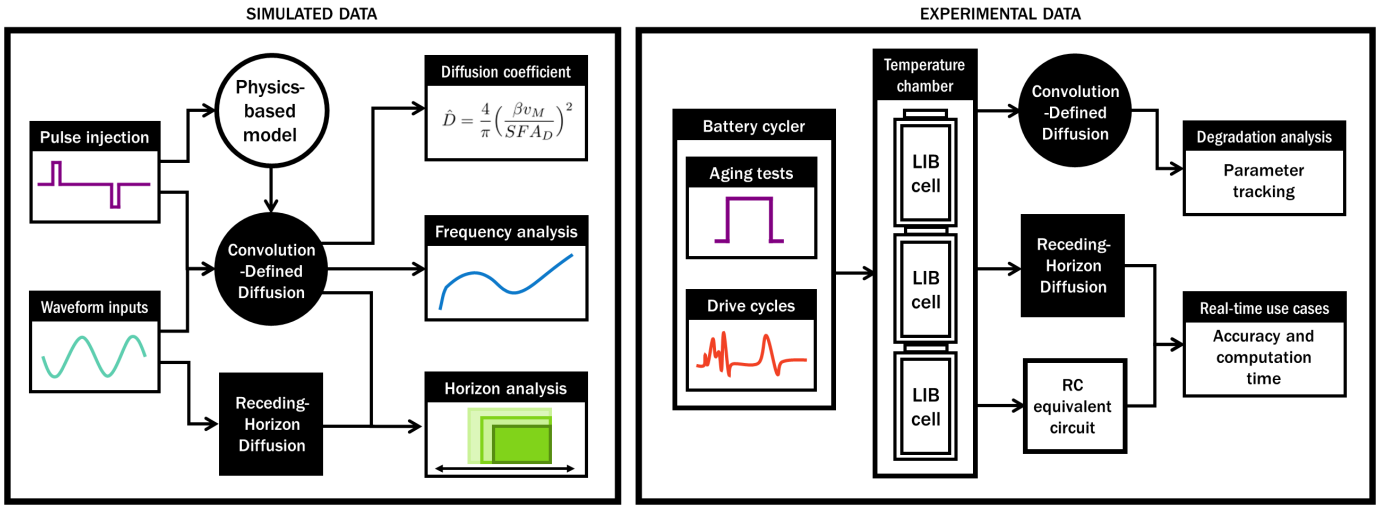

Fig. 3. Overview of simulated and experimental setup for data collection and analysis

$$A_\nu = \begin{pmatrix} 1 & a_M & 0 & 0 & 0 & \cdots & 0 \\ 0 & 0 & a_M & 0 & 0 & \cdots & 0 \\ 0 & 0 & 0 & a_{M-1} & & & 0 \\ 0 & 0 & 0 & 0 & \ddots & & \vdots \\ \vdots & \vdots & \vdots & \vdots & & a_2 & 0 \\ 0 & 0 & 0 & 0 & \cdots & 0 & a_1 \\ 0 & 0 & 0 & 0 & \cdots & 0 & 0 \end{pmatrix} \tag{23}$$

$$B_\nu = \begin{pmatrix} \mathbf{0} \\ \vdots \\ \mathbf{0} \\ b_\nu(t_k) \end{pmatrix}, \quad C_\nu = A_D \begin{pmatrix} 1 & \cdots & 1 & 1 \end{pmatrix}$$

where $x_\nu \in \mathbf{R}^{M+2}$ is a column vector, $A_\nu \in \mathbf{R}^{(M+2)\times(M+2)}$ is a square matrix, $B_\nu(k) \in \mathbf{R}^{(M+2)\times 2}$ is a matrix with $M+2$ rows and 2 columns, $C_\nu \in \mathbf{R}^{M+2}$ is a row vector, x_{offset} is a scalar, and a_m is a scalar derived from (18),

$$a_m = \sqrt{1 + \frac{1}{m}} \tag{24}$$

The parameter A_D in C_ν is the only modelling parameter that must be identified. The step horizon M is treated as a tuning parameter that is fixed before implementation of the RHD model. Step horizon corresponds to a length of time, so for a 10s horizon and a sampling interval of 0.1 s, $M = 100$.

Dynamic processes occur in the state vector due to the off-diagonal of the matrix A_ν. At each k, A_ν advances the states to the next time step. One state saturates and another is initialized. Saturated states are stored in the offset term x_{offset} accumulating the effects of OCV change. In contrast to the CDD model, the RHD model only requires a fixed number of states that are updated recursively in discrete-time. Thus a completely linear state-space definition is achieved.

IV. Verifying Convolution-Defined Diffusion

The first link between CDD and diffusion is demonstrated with PBM-simulated data. Unlike in real systems, the aggregated diffusion coefficient of the cell is known in a PBM. Thus the CDD-predicted diffusivity $\hat{D}$ may be calculated from the diffusion constant A_D and the known PBM parameters,

$$\hat{D} = \frac{4}{\pi}\left(\frac{\beta v_M}{SFA_D}\right)^2 \tag{25}$$

where the parameters are defined in Table I and $1/\beta = 0.55$, $\varepsilon_{AM} = 0.306$, and $L_{agg} = 1\,\mu$m. The prediction $\hat{D}$ is then compared with the true model diffusivity. Simulations of pulse perturbation are performed using varied diffusion coefficients in a coupled agglomerate-scale and electrode-scale continuum PBM for an NMC cell, described in [23], [24], with SoC range [0.16, 0.90] and SoH range [0.61, 1]. For simplicity, the PBM does not capture charge transfer dynamics so the only CDD parameters are R_0 and A_D, hence the name 'CDD-0RC'. Parameter estimation is performed using the scatter-search non-linear global optimization algorithm [7], [25].

Results are shown in Fig. 4 with simulated voltage shown in 4a. The mean absolute percent error (MAPE) of the predicted voltage is bounded by 1% for all pulses. The highest error results from low diffusivities and high SoC which may cause OCV dynamics not captured by the diffusion overpotential. Besides these extremes, the CDD model accurately models the PBM voltage response. The prediction trendline demonstrates strong agreement with the true diffusivity. Individual diffusivity may vary due to SoC-varying initial states such as the initial concentration of lithium-ions. Still, the CDD model diffusion constant A_D is a good indicator of the internal diffusivity.

The second link to the diffusion overpotential is from frequency analysis of CDD-simulated data. In electrochemical impedance spectroscopy, the overpotentials are clearly observed in the frequency domain Nyquist curves [9]. Only diffusion is known to affect the low-frequency 'tail'. Therefore the frequency spectrum of the simulated CDD model should yield distinct behavior in the Nyquist curves. Frequency analysis of simulated CDD model data is performed by calculating the complex frequency-varying impedance $Z(s)$, obtained using simulated pulse impedance spectroscopy, detailed in [26]. To observe the effects of R_0, R_1, and A_D, one parameter is varied while the others are held constant. This allows the frequency

This article has been accepted for publication in IEEE Transactions on Transportation Electrification. This is the author's version which has not been fully edited and content may change prior to final publication. Citation information: DOI 10.1109/TTE.2023.3238282

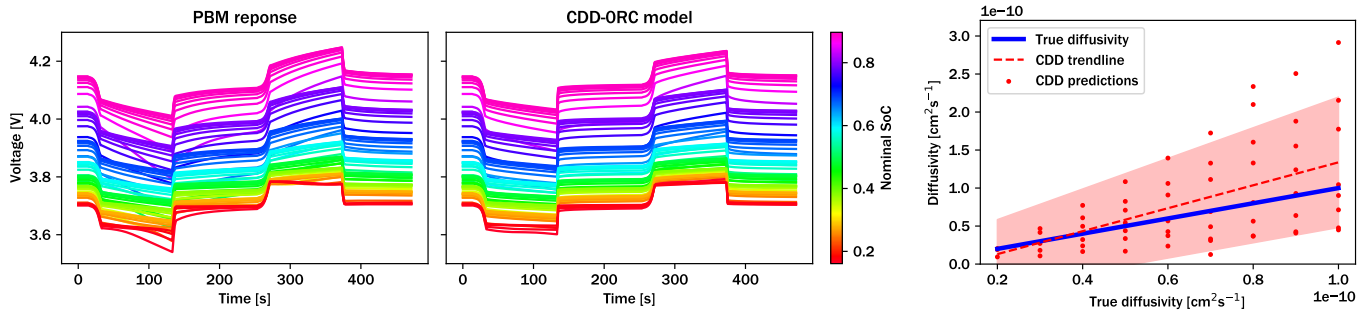

(a) (b)

Fig. 4. Comparison between the CDD-0RC model and PBM model, showing (a) PBM-simulated voltage response and predicted CDD-0RC voltage and (b) Apparent diffusivity predicted by CDD-0RC model compared with the true PBM diffusivity.

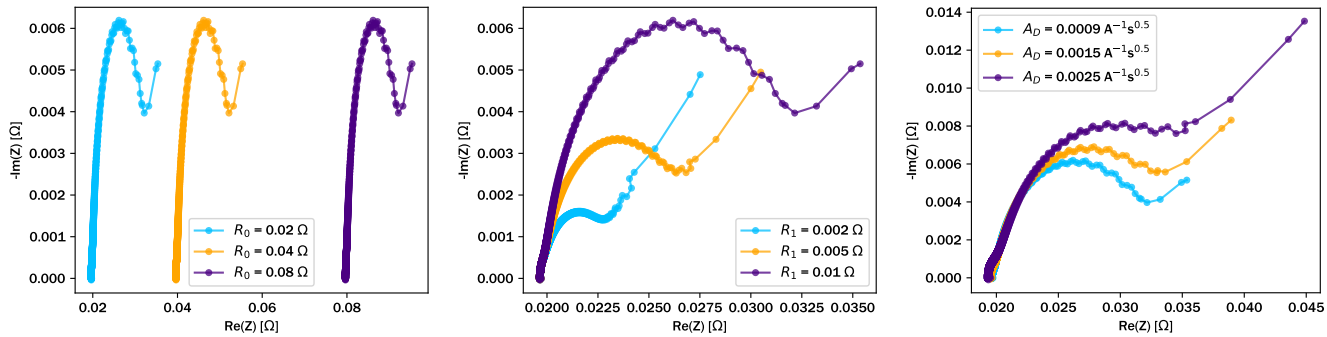

(a) (b) (c)

Fig. 5. Nyquist curves from frequency analysis of simulated CDD-1RC time-domain data, showing overpotential variations in (a) Ohmic, (b) Charge transfer, and (c) Diffusion

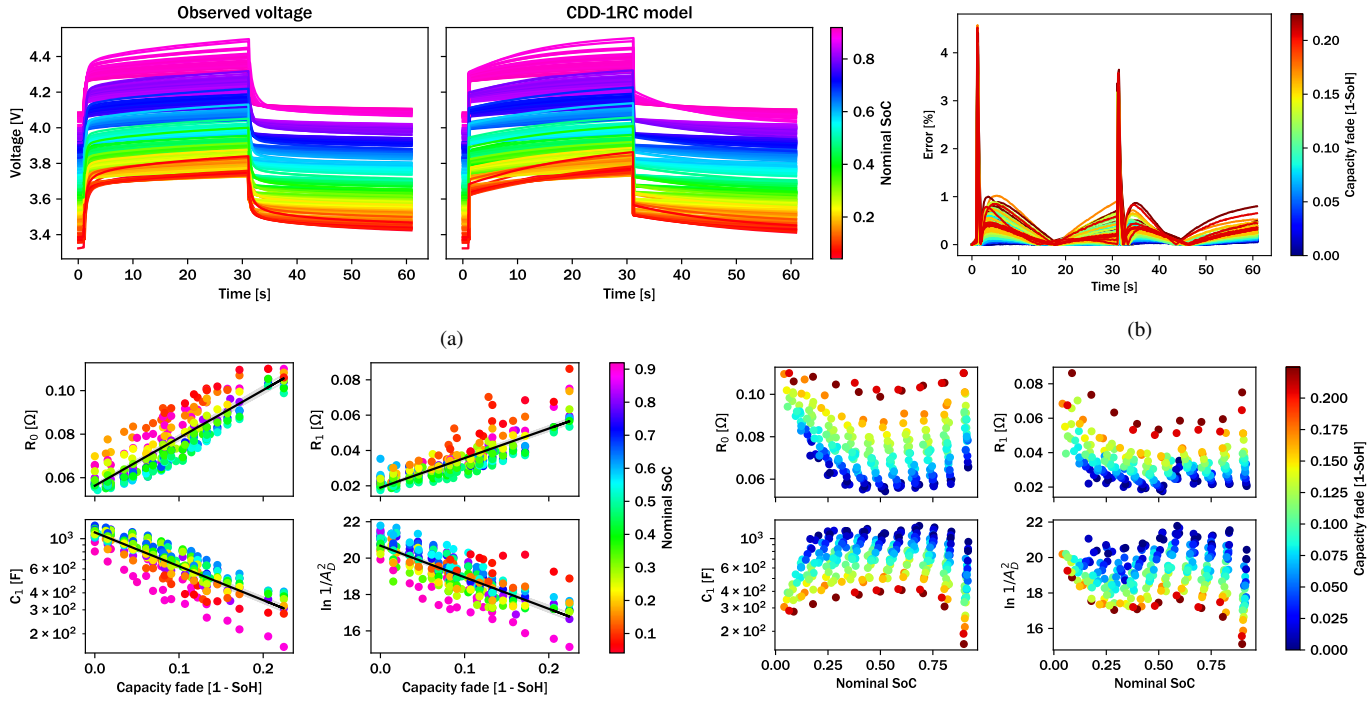

(a) (b) (c) (d)

Fig. 6. Analysis of aged NMC cells at various SoC using the CDD-1RC model, showing (a) observed cell voltage and predicted CDD-1RC voltage, (b) Absolute percent error of the predicted voltage color-coded by SoH, and (c)-(d) CDD-1RC modelling parameters plotted against SoH and SoC

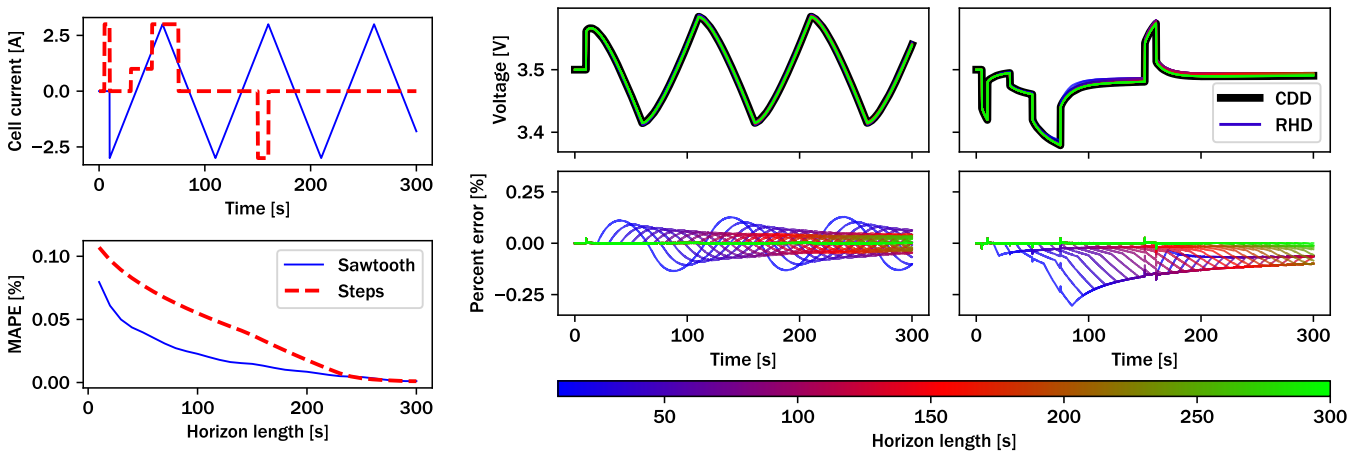

(a) (b)

Fig. 7. Results showing how RHD approximates CDD, with (a) Simulated current waveforms and variation of voltage MAPE between RHD and CDD, and (b) Voltage and percent error using various RHD horizon lengths (in color) compared with the CDD output (in black)

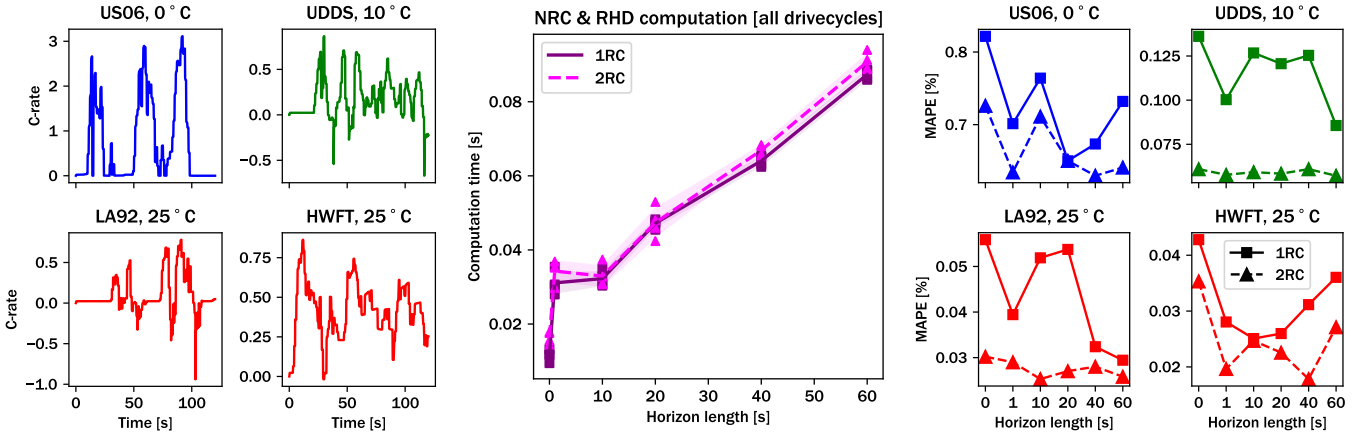

(a) (b) (c)

Fig. 8. Comparison between proposed RHD model and NRC models, showing (a) Drive cycle data, (b) Computation time, and (c) MAPE for various horizon lengths. Horizon length 0 refers to the NRC model, and non-zero horizon refers to the RHD model

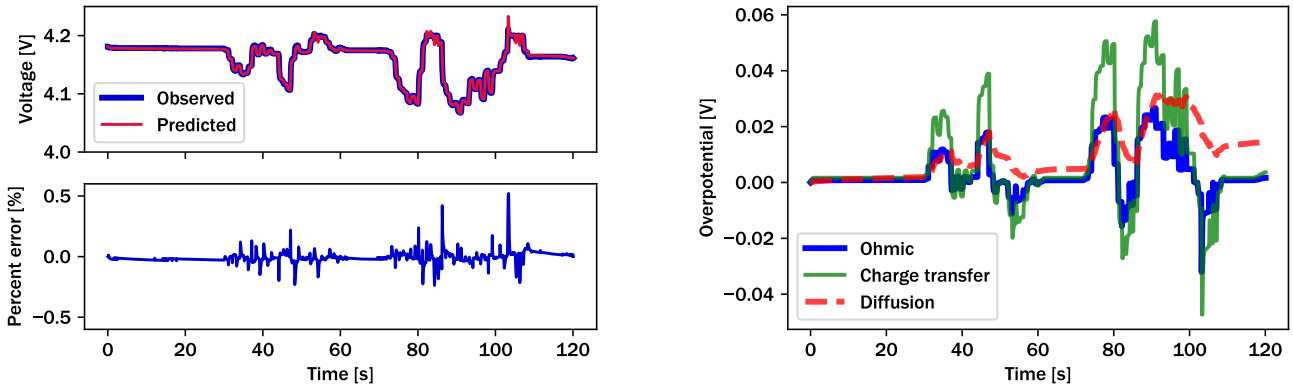

(a) (b)

Fig. 9. Overpotential analysis for LA92 data using RHD-1RC model with a 20 s horizon, showing (a) Voltage prediction and percent error and (b) Variation of overpotentials over time

behavior to be clearly observed. Results are shown in Fig. 5. It can be seen that the parameters affect the Nyquist plot as expected. Ohmic resistance R_0 shifts the x-axis crossing, R_1 affects the size of the mid-frequency semi-circle, and A_D affects the low-frequency tail, again suggesting that A_D is uniquely linked to diffusion.

The third validation uses experimental aging data to demonstrate how the CDD model can track cell parameters over the cell's lifetime. This is important for cell diagnostics. Different usage profiles may result in different parameter trends, which can inform optimal cell cycling conditions. Experimental cell aging data is collected from 3 commercial 2.7 Ah lithium NMC oxide cells (Panasonic NCR18650PF) held at 10°C. Cycling protocol is similar to the procedure described in [27]. Cells are degraded by low-voltage cycling at 1 C-rate, which can represent incomplete charging and high depth-of-discharge. This usage profile could be common in portable electronics. There are 14 unique state of health (SoH) in the range [0.78, 1]. At each SoH, unipolar charge pulses are applied to the cell at SoC in the range [0.04, 0.92]. The CDD-1RC model parameters are then estimated from the voltage responses.

Results for the cell lifetime are shown in Fig. 6. Percent error in Fig. 6b spikes at transitions, but otherwise remains low. On average, the MAPE of each pulse is below 0.5%. There are very strong trends in the CDD-1RC parameters, shown in Figs. 6c-d. Resistances increase as SoH decreases, while capacitance decreases. The diffusion constant A_D, which varies inversely with diffusivity, is seen to increase as SoH decreases. This agrees with the observations in [28], where lithium-ion diffusion may be slowed by degradation processes.

V. Verifying Receding-Horizon Diffusion

Having validated CDD, we now show that RHD exactly approximates CDD for a sufficient horizon length. Simulations of the RHD and CDD model are compared to demonstrate how the receding horizon approximates convolution. Two voltage waveforms are simulated for comparison: sawtooth and current steps. Identical parameters are used in the 2RC-pair models but the RHD horizon length is varied from 10s to 300s. The horizon-length-varying error between the RHD approximation and CDD simulation is then examined for both waveforms.

Results are shown in Fig. 7. Approximation error decreases to zero as the horizon length approaches the data length of 300 s. The sawtooth wave is approximated more accurately than current steps. This suggests that the RHD model is slightly more suited to inputs with constant non-zero gradients, which is often the case in real systems. Approximation error is small regardless of the input. Rather than require the entire current input to be known a posteriori, the RHD model only requires two samples of the input and a fixed number of states for a highly accurate discrete-recursive approximation of convolution.

Experimental drive cycle data is used to compare real-time RHD model performance to that of conventional NRC models. Data is obtained from [29], where a fresh 2.9 Ah nickel-cobalt-aluminum cell (Panasonic 18650PF) is tested in a thermal chamber. The four drive cycles, summarized in Table II, were applied in two-minute portions, sampled at 10 Hz, to the fully rested cell, shown in Fig. 8a. Computation time and MAPE of the RHD model were then assessed.

TABLE II
Drive cycle specifications.

Name	[°C]	Description
US06	0	High-acceleration driving
UDDS	10	Urban dynamometer driving schedule
HWFT	25	Highway fuel economy test
LA92	25	California-centric

Results for computation time and error using the drive cycles are shown in Figs. 8b and 8c. RHD models have higher computation time due to the larger state vector, but computation time is traded-off for accuracy. When the RHD model is used (indicated by non-zero horizon-length), the MAPE is consistently lower than or bounded by the NRC (0-horizon) error. This shows that the proposed diffusion element increases modelling accuracy. The exact improvement is most easily observed for the 1 RC-pair models, and is data-dependent. For the lower current cycles, UDDS and LA92, error decreases with the horizon length. In contrast, the optimal horizon length for US06 and HWFT cycles is around 40 s. This could reflect real-life LIB diffusion processes, which have time-constants of similar orders [20].

The second use of drive cycle data is for tracking overpotentials. Results of overpotential analysis using the LA92 drivecyle are shown in Fig. 9 for the RHD-1RC with a 40 s horizon. Maximum error is less than 0.51%. Overpotentials are easily disaggregated from the predicted voltage, showing that different processes dominate at different times. This agrees with results in [30]. Further investigations could use these results to evaluate the dominant overpotential in different scenarios, giving insight into limiting transport phenomena.

Now that the CDD and RHD model have been validated, there is even more choice in battery models for modelling transport kinetics. Table III summarizes the key features of NRC, Randles-Warburg, FOM, CDD, and RHD models. It shows how the charge transfer and diffusion overpotentials are defined, the mathematical formulation, and whether they are preferred for the frequency f or time t domains. It can be seen that our models strike a balance between the NRC, Randles, and FOM models— they avoid fractional calculus, have a single interpretable diffusion constant, and can be used in the time-domain.

VI. Conclusion

We have studied diffusion in LIB cells using physically-interpretable time-domain ECMs. We show that the diffusion overpotential may be captured using convolution and name this the CDD model. RHD is then shown to approximate the CDD with high fidelity using a fixed-size discrete-time recursive state-space system. RHD is the first representation of diffusion to use a single modelling parameter without fractional-order calculus. Verification using simulated and experimental data shows that the RHD model is fast, accurate, and general-purpose compared to RC-pair circuits. It could be easily

TABLE III
COMPARISON BETWEEN EQUIVALENT CIRCUIT MODELS.

Model	Charge transfer	Diffusion	Formulation	Domain
NRC	RC pairs	RC pairs	Linear state-space	t
Randles	RC pairs	A_W	Transfer function	f
FOM	CPE	A_W	Fractional calculus	f
CDD	RC pairs	A_D	Convolution	t
RHD	RC pairs	A_D	Linear state-space	t

adapted to existing BMS state estimation techniques such as Kalman filters to offer further insight into battery degradation.

Further validation and model optimization may be needed. More extreme temperatures and current rates can be applied. Subsampling techniques could be used to reduce the size of the diffusion state vector. Finally, the RHD model can be integrated with advanced diagnostics in a real EV or grid system. This could give a greater understanding of internal cell dynamics with small increases in computation time.

REFERENCES

[1] S. Yang, Z. Zhang, R. Cao, M. Wang, H. Cheng, L. Zhang, Y. Jiang, Y. Li, B. Chen, H. Ling, Y. Lian, B. Wu, and X. Liu, "Implementation for a cloud battery management system based on the chain framework," *Energy and AI*, vol. 5, no. 100088, 2021.

[2] A. Carnovale and X. Li, "A modeling and experimental study of capacity fade for lithium-ion batteries," *Energy and AI*, vol. 2, no. 100032, 2020.

[3] K. S. Mayilvahanan, J. Kuang, A. H. McCarthy, L. Wang, K. J. Takeuchi, A. M. Marschilok, E. S. Takeuchi, and A. C. West, "Understanding evolution of lithium trivanadate cathodes during cycling via reformulated physics-based models and experiments," *J. Electrochem. Soc.*, vol. 168, no. 050525, 2021.

[4] A. G. Li, , A. C. West, and M. Preindl, "Towards unified machine learning characterization of lithium-ion battery degradation across multiple levels: A critical review," *Appl. Energy*, vol. 316, no. 119030, 2022.

[5] J. Tian, R. Xiong, , W. Shen, J. Wang, and R. Yang, "Online simultaneous identification of parameters and order of a fractional order battery model," *J. Cleaner Production*, vol. 247, no. 119147, 2020.

[6] Y. Li, T. Wik, C. Xie, Y. Huang, B. Xiong, J. Tang, and C. Zou, "Control-oriented modeling of all-solid-state batteries using physics-based equivalent circuits," *IEEE Trans. Tranp. Elec.*, vol. 8, no. 2, 2022.

[7] A. G. Li, K. Mayilvahanan, A. C. West, and M. Preindl, "Discrete-time modeling of li-ion batteries with electrochemical overpotentials including diffusion," *J. Power Sources*, vol. 500, no. 229991, 2021.

[8] J. Xu, C. C. Mi, B. Cao, and J. Cao, "A new method to estimate the state of charge of lithium-ion batteries based on the battery impedance model," *J. Power Sources*, vol. 233, pp. 277–284, 2013.

[9] N. Meddings, M. Heinrich, F. Overney, J. Lee, V. Ruiz, E. Napolitano, S. Seitz, G. Hinds, R. Raccichini, M. Gaberscek, and J. Park, "Application of electrochemical impedance spectroscopy to commercial li-ion cells: A review," *J. Power Sources*, vol. 480, no. 228742, 2020.

[10] U. Krewer, F. Roder, E. Harinath, R. D. Braatz, B. Bedurftig, and R. Findeisen, "Review—dynamic models of li-ion batteries for diagnosis and operation: A review and perspective," *J. Electrochem. Soc.*, vol. 165, no. 16, pp. A3656–A3673, 2018.

[11] K. S. Cole and R. H. Cole, "Dispersion and absorption in dielectrics I. alternating current characteristics," *J. Chemical Physics*, vol. 9, no. 341, 1941.

[12] Z. Liu, Y. Qiu, J. Feng, S. Chen, and C. Yang, "A simplified fractional order modeling and parameter identification for lithium-ion batteries," *J. Electrochem. En. Conv. Stor.*, vol. 19, no. 021001, 2021.

[13] S. M. M. Alavi, C. R. Birkl, and D. A. Howey, "Time-domain fitting of battery electrochemical impedance models," *J. Power Sources*, vol. 288, pp. 345–352, 2015.

[14] A. Nasser-Eddine, B. Huard, J. D. Gabano, T. Poinot, S. Martemianov, and A. Thomas, "Fast time domain identification of electrochemical systems at low frequencies using fractional modeling," *J. Electroanalytical Chemistry*, vol. 862, no. 113967, pp. 345–352, 2020.

[15] J. Tian, R. Xiong, and Q. Yu, "Fractional-order model-based incremental capacity analysis for degradation state recognition of lithium-ion batteries," *IEEE Trans. Industrial Electronics*, vol. 68, no. 2, 2019.

[16] H. Ekstrom, B. Fridhom, and G. Lindbergh, "Comparison of lumped diffusion models for voltage prediction of a lithiumion battery cell during dynamic loads," *J. Power Sources*, vol. 402, pp. 296–300, 2018.

[17] C. Brivio, V. Musolino, M. Merlo, and C. Ballif, "A physically-based electrical model for lithium-ion cells," *IEEE Trans. Energy Conversion*, vol. 34, no. 2, 2019.

[18] C. Cheng, H. S. Chung, R. W. Lau, and K. Y. Hong, "Time-domain modeling of constant phase elements for simulation of lithium battery behavior," *IEEE Trans. Power Elec.*, vol. 34, no. 8, 2019.

[19] C. Li, N. Cui, Z. Cui, C. Wang, and C. Zhang, "Novel equivalent circuit model for high-energy lithium-ion batteries considering the effect of nonlinear solid-phase diffusion," *J. Power Sources*, vol. 523, no. 230993, 2022.

[20] S. Gantenbein, M. Weiss, and E. Ivers-Tiffé, "Impedance based time-domain modeling of lithium-ion batteries: Part i," *J. Power Sources*, vol. 379, pp. 317–327, 2018.

[21] W. Weppner and R. A. Huggins, "Determination of the kinetic parameters of mixed-conducting electrodes and application to the system Li3Sb," *J. Electrochem. Soc.*, vol. 124, no. 10, pp. 1569–1578, 1977.

[22] D. Guo, G. Yang, X. Feng, X. Han, L. Lu, and M. Ouyang, "Physics-based fractional-order model with simplified solid phase diffusion of lithium-ion battery," *J. Energy Storage*, vol. 30, no. 101404, 2020.

[23] N. W. Brady, Q. Zhang, A. Bruck, D. C. Bock, C. A. Gould, A. C. Marschilok, K. Takeuchi, E. Takeuchi, and A. C. West, "Operando study of LiV3O8 cathode: Coupling EDXRD measurements to simulations," *J. Electrochem. Soc.*, vol. 165, no. 2, pp. A371–A379, 2018.

[24] Z. Hui, K. S. Mayilvahanan, Y. Yang, and A. C. West, "Determining the length scale of transport impedances in li-ion electrodes: Li(Ni0.33Mn0.33Co0.33)O2," *J. Electrochem. Soc.*, vol. 167, no. 100542, 2020.

[25] Z. Ugray, L. Lasdon, J. Plummer, F. Glover, J. Kelly, and R. Marti, "Scatter search and local nlp solvers: A multistart framework for global optimization," *INFORMS Journal on Computing*, vol. 19, no. 3, pp. 328–340, 2007.

[26] A. G. Li, M. M. Wu, Y. A. Fahmy, and M. Preindl, "Fast time-domain impedance spectroscopy of lithium-ion batteries using pulse perturbation," *IEEE Transportation Electrification Conference (ITEC)*, 2022.

[27] A. G. Li, W. Wang, A. C. West, and M. Preindl, "Health and performance diagnostics in li-ion batteries with pulse-injection-aided machine learning," *Appl. Energy*, vol. 315, no. 119005, 2022.

[28] Y. Preger, H. M. Barkholtz, A. Fresquez, D. L. Campbell, B. W. Juba, J. Roman-Kustas, S. R. Ferreira, and B. Chalamala, "Degradation of commercial lithium-ion cells as a function of chemistry and cycling conditions," *J. Electrochem. Soc.*, vol. 167, no. 120532, 2020.

[29] P. Kollmeyer, "Panasonic 18650pf li-ion battery data," *Mendeley Data, V1*, no. 101404, 2018.

[30] V. J. Ovejas and A. Cuadras, "State of charge dependency of the overvoltage generated in commercial Li-ion cells," *J. Power Sources*, vol. 418, pp. 176–185, 2019.